https://doi.org/10.5194/egusphere-2026-829
Preprint. Discussion started: 4 March 2026

Increasing heat stress across Southeast Asia driven by compound warming and moistening

Dzung Nguyen–Le*[1]

Email: nguyen-le.dung@usth.edu.vn; ORCID: 0000-0003-0214-3411

* Corresponding author

[1]Department of Space and Earth Sciences, University of Science and Technology of Hanoi (USTH), Vietnam Academy of Science and Technology (VAST), Hanoi, Vietnam

(A manuscript for submission to *Natural Hazards and Earth System Sciences*, February 2026)

https://doi.org/10.5194/egusphere-2026-829
Preprint. Discussion started: 4 March 2026

Abstract

Heat stress is intensifying across Southeast Asia under global warming, yet the relative influences of atmospheric warming and moistening across timescales remain insufficiently quantified. This study investigates the thermodynamic drivers of warm-season (April–October) heat-stress intensity, measured by the daily maximum wet-bulb globe temperature (*WBGTmax*), and frequency, defined as the annual number of extreme heat-stress days (*Nxday*), across Southeast Asia and its 20 climatic sub-regions. Using observations together with dynamically downscaled CORDEX–SEA simulations, we apply a unified attribution framework to separate the effects of air temperature, specific humidity, and residual nonlinear processes on historical (1985–2014) trends, interannual variability, and projected late-century changes (2071–2100 relative to 1985–2014) under SSP5–8.5. Historical increases in *WBGTmax* and *Nxday* are dominated by temperature across much of the region. However, humidity already provides important amplification in monsoon-influenced lowlands, including Indochina, the Philippines, and parts of the Malay Peninsula. Future projections indicate a coherent basin-wide shift toward compound warm–humid conditions. In many monsoon regions, rising moisture contributes roughly 30–50 % of the increase, consistent with enhanced atmospheric water-holding capacity in a warmer climate. In contrast, interannual variability, particularly over the Maritime Continent, is strongly governed by nonlinear temperature–humidity interactions, which generate substantial unexplained components. Because *Nxday* depends on threshold exceedance, it shows a stronger amplification of future change than *WBGTmax*, even though its long-term evolution remains primarily temperature controlled. Overall, the results demonstrate that heat-stress escalation in Southeast Asia increasingly reflects rising atmospheric moist enthalpy rather than dry-bulb warming alone, underscoring the need for adaptation strategies that explicitly consider both temperature and humidity.

Keywords: *heat stress*; *wet-bulb globe temperature (WBGT)*; *global warming*; *temperature–humidity interactions*; *thermodynamic decomposition*; *Southeast Asia*.

https://doi.org/10.5194/egusphere-2026-829
Preprint. Discussion started: 4 March 2026

1. Introduction

Southeast Asia (SEA), situated in the tropical Asia–Pacific region, includes both mainland and maritime territories of eleven countries and is home to more than 700 million people. The climate is characterized by persistently high temperature and humidity, with rainfall strongly regulated by the Asian monsoon system (Räsänen et al., 2016). Despite its broadly tropical setting, SEA exhibits pronounced spatial contrasts and strong seasonality in both precipitation and temperature due to interactions among large-scale circulation, land–sea thermal contrasts, and complex topography (Chang et al., 2005; Juneng et al., 2016). To better represent this diversity, SEA has been partitioned into 20 climatic sub-regions within the SEA regional climate downscaling/coordinated regional climate downscaling experiment–SEA (SEACLID/CORDEX–SEA) project (Juneng et al., 2016; Cruz et al., 2017; Tangang et al., 2020).

SEA is widely regarded as one of the regions most exposed to climate change impacts (Collins et al., 2013), while mitigation and adaptation capacities vary substantially among countries (Overland et al., 2021). Among climate-related hazards, increasing heat stress presents serious threats to public health, outdoor labor, and economic productivity (Barriopedro et al., 2011; Dunne et al., 2013; Kjellstrom et al. 2016, 2018). In contrast to many mid-latitude regions, where extreme heat stress is often dominated by dry-bulb temperature, heat stress in SEA is strongly governed by the combined influence of air temperature and atmospheric moisture (e.g., Zhou et al., 2024; Kushwaha et al., 2026). The wet-bulb globe temperature (WBGT) is therefore widely used to quantify human heat exposure, particularly in climate-change studies, as it explicitly captures this thermodynamic coupling between temperature, humidity, radiation, and wind (Yaglou and Minard, 1957, De Freitas and Grigorieva, 2007).

Consistent increases in WBGT have been reported under global warming at both global and regional scales (e.g., Im et al., 2017, Lee and Min, 2018; Schwingshackl et al., 2021, Mohammad and Weng, 2025, Kushwaha et al., 2026). However, the relative importance of rising temperature

https://doi.org/10.5194/egusphere-2026-829
Preprint. Discussion started: 4 March 2026

versus increasing atmospheric moisture remains insufficiently constrained. Quantifying these contributions is essential for adaptation planning, since temperature-dominated heat stress favors strategies such as shading or insulation, whereas humidity-driven stress highlights the need for ventilation and the limits of evaporative cooling. Furthermore, the mechanisms governing long-term changes may differ from those responsible for interannual variability. While anthropogenic forcing produces a persistent warming trend, climate mode such as the El Niño–Southern Oscillation (ENSO) can strongly modulate regional moisture conditions, generating short-lived yet intense heat stress anomalies (Raymond et al., 2020). This issue is particularly relevant for SEA, where ENSO teleconnections exert a major control on regional hydroclimate (Nguyen-Le, 2024).

SEA thus provides a valuable setting for investigating the thermodynamic controls of heat stress. The maritime environment maintains high background humidity, meaning that relatively small temperature increases can drive WBGT toward thresholds critical for human tolerance (Buzan and Huber, 2020). Although many studies have assessed projected changes in heat stress magnitude (e.g. Manimaran et al., 2025; Nguyen-Le et al., 2026), fewer have systematically separated the effects of temperature and moisture or compared the drivers of mean-state change with those of interannual variability across spatial scales.

This study addresses that gap by quantifying the respective roles of near-surface air temperature (T) and specific humidity (q) in shaping heat stress across SEA. We analyze the historical period (1985–2014) and late-century projections (2071–2100) under the SSP5–8.5 scenario (Eyring et al., 2016; O'Neill et al., 2017 using observations together with dynamically downscaled CORDEX–SEA simulations. A unified attribution framework is applied to evaluate contributions of T and q to (1) historical trends, (2) interannual variability, and (3) climatological mean-state changes between historical and future climates. The results provide spatially explicit insight into where and why WBGT changes occur, offering information relevant for risk assessment and adaptation planning across SEA and its 20 climatic sub-regions.

https://doi.org/10.5194/egusphere-2026-829
Preprint. Discussion started: 4 March 2026

The remainder of the paper is organized as follows. Section 2 describes the study region, datasets, WBGT estimation, and attribution methods. Section 3 presents the results, and Section 4 concludes with discussion and implications.

2. Study region, datasets, and methodology

2.1 Study region

Figure 1 shows the SEA domain (12° S–27.5° N, 90° E–145° E) and the 20 climatic sub-regions defined by Juneng et al. (2016). Although much of SEA lies within the tropical belt, where annual mean temperature typically exceeds 25 °C, substantial sub-regional contrasts in circulation and rainfall lead to marked differences in humidity and, consequently, heat-stress conditions.

In the northern part of SEA, including northern Indochina (R18–R19), Myanmar (R20), and the Philippines (R01–R02), boreal-winter and early spring northeasterly cold surges from East Asia bring episodic cooling and drying (Chang et al., 2005), temporarily reducing heat stress. During the remainder of the year, precipitation becomes the primary control on moisture availability and thus on the seasonal evolution of heat stress. Mainland SEA (R15–R20) and the Philippines are strongly influenced by the Asian summer monsoon (Matsumoto 1997; Wang and LinHo 2002; Nguyen-Le 2023). During boreal summer, enhanced humidity substantially intensifies heat stress even where temperature variations are modest. Over much of the Maritime Continent (R04–R12), peak rainfall instead occurs during the boreal winter monsoon (Juneng et al. 2016), sustaining high humidity and favoring near year-round heat exposure. Other areas, including Borneo (R03), western Malaysia (R13), and northern Sumatra (R14), experience rainfall maxima during boreal autumn (Nguyet-Le 2023). In these locations, the concurrence of elevated humidity and persistently high temperature produces pronounced seasonal peaks in moist heat stress.

https://doi.org/10.5194/egusphere-2026-829
Preprint. Discussion started: 4 March 2026

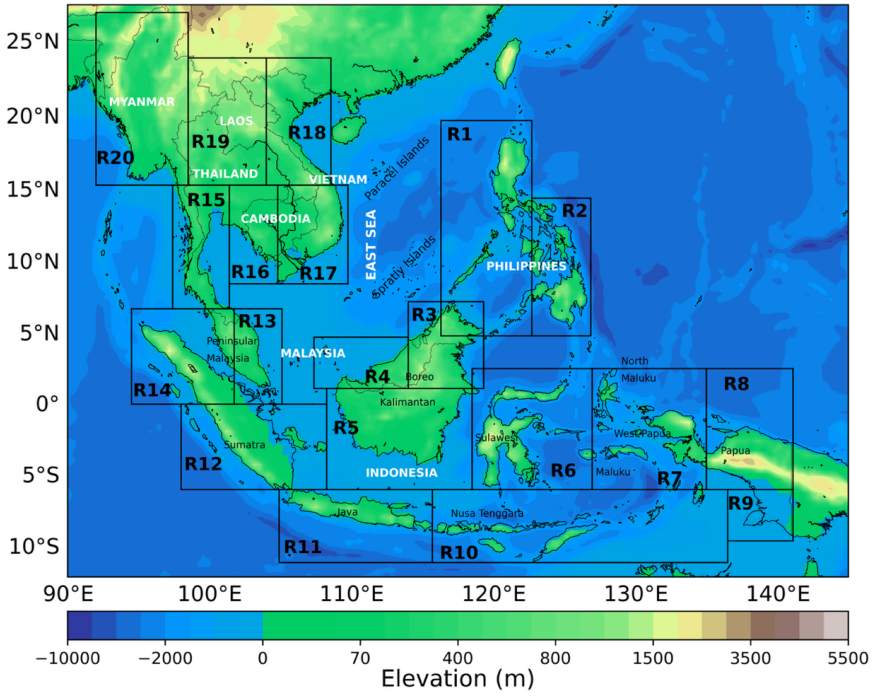

Figure 1: Southeast Asia (SEA) domain and its 20 climatic sub-regions (outlined by black boxes) following the SEACLID/CORDEX–SEA framework. Shading indicates topography from the Global 30 Arc-Second Elevation (GTOPO30) dataset (EROS, 2017).

2.2 Heat-stress indices and thresholds

Heat stress is evaluated using the wet-bulb globe temperature (WBGT), a composite index that integrates the effects of air temperature, atmospheric moisture, wind speed, and radiative heat load. WBGT has been widely applied in occupational health and climate-impact assessments because it provides a direct measure of environmental constraints on human thermoregulation (De Freitas and Grigorieva, 2007).

WBGT is formulated as a weighted combination of the natural wet-bulb temperature (T_w), black globe temperature (T_g), and dry bulb temperature (T_a). T_w represents evaporative cooling under ambient conditions and depends mainly on temperature and humidity. T_g reflects radiative heat gain from shortwave and longwave fluxes and is additionally influenced by wind speed. T_a corresponds to

https://doi.org/10.5194/egusphere-2026-829
Preprint. Discussion started: 4 March 2026

the shaded air temperature. For outdoor daytime environments with solar exposure, WBGT is defined as

$$WBGT_{outdoor} = 0.7T_w + 0.2T_g + 0.1T_a \quad (1)$$

where the weighting emphasizes the dominant role of evaporative cooling limitations in determining heat strain.

Because boreal-winter cold surges substantially reduce heat stress across large parts of Southeast Asia, the analysis concentrates on the warm season from April to October. WBGT is calculated following the physically based heat-balance model of (2008), implemented using the open-source Python framework described by Kong and Huber (2022). Heat-stress intensity is represented by *WBGTmax*, defined as the daily maximum value of outdoor WBGT (Equation 1).

Table 1. Summary of wet-bulb globe temperature (WBGT) Thresholds (Based on ISO 7243:2017).

Risk Level	WBGT Threshold	Work/Rest Allocation	ISO 7243:2017 Context
Level 1	28 °C	100% Work	**Reference Limit (Moderate Work):** Safe for sustained 8-hour moderate labor.
Level 2	30 °C	50% Work / 50% Rest	**Action Limit:** Maximum limit for light work; requires 30 min rest/hour for moderate work.
Level 3	32 °C	25% Work / 75% Rest	**High Strain:** Severe risk for moderate labor; requires dominant rest periods.
Level 4	>33 °C	No sustained work	**Ceiling:** Threshold where environmental heat exceeds human cooling capacity for labor.

Changes in heat-stress indices alone do not fully capture societal impacts, as their relevance depends on physiologically meaningful thresholds. To translate climatic changes into implications for human health and labor productivity, we adopt guidance from ISO 7243:2017, which links

https://doi.org/10.5194/egusphere-2026-829
Preprint. Discussion started: 4 March 2026

WBGT levels to physiological strain and work–rest requirements (ISO 2017). An extreme heat-stress day is defined as a day on which *WBGTmax* exceeds 30 °C. This threshold corresponds to the upper reference limit for light manual work and a level of high physiological strain for moderate work, at which allowable work time typically must be reduced by about 50% per hour to maintain core body temperature below 38 °C. Heat-stress frequency is quantified using *Nxday*, defined as the annual number of extreme heat-stress days.

Atmospheric moisture is represented by specific humidity (q) rather than relative humidity, which is commonly used in heat-stress analyses (e.g. Zhou *et al.* 2024). Specific humidity q is preferred because it is a conserved thermodynamic variable and allows a clearer physical separation between temperature-driven and moisture-driven influences on WBGT. In contrast, relative humidity is strongly dependent on T and often shows limited change under global warming (Douville et al., 2022), which can obscure attribution of the underlying drivers.

2.3 Datasets and preprocessing

Historical heat stress is evaluated using the ECMWF (European Centre for Medium-Range Weather Forecasts) ERA5 reanalysis (Hersbach *et al.* 2020) for 1985–2014. Future conditions are derived from regional climate projections produced within CORDEX–SEA (Tangang et al., 2020; Ngo-Duc et al., 2024), which dynamically downscale simulations from Coupled Model Intercomparison Project (CMIP6; Eyring et al., 2016) to a horizontal resolution of 25 km.

Two driving global climate models, NorESM2-MM and CNRM-ESM2-1, are dynamically downscaled using the non-hydrostatic RegCM4-NH regional climate model (Coppola et al., 2021). Model T, q, wind speed, surface pressure, and radiative fluxes are archived at 3-hourly interval. . For consistency with the observational reference, all variables are interpolated onto the 0.25° ERA5 grid prior to WBGT calculation.

https://doi.org/10.5194/egusphere-2026-829
Preprint. Discussion started: 4 March 2026

Although projections are available for multiple Shared Socioeconomic Pathways (SSP1–2.6, SSP2–4.5, and SSP5–8.5) covering 1985–2100, the present analysis emphasizes late-century change (2071–2100) under SSP5–8.5 in order to characterize upper-bound heat-stress risk.

Systematic model biases are adjusted using the multivariate bias-correction method based on N-dimensional probability density functions (MBCn). The correction is applied individually to T, q, wind speed, surface pressure, and shortwave radiation for each regional simulation. By preserving inter-variable dependence, this approach improves consistency in compound indices such as WBGT, which depend jointly on thermodynamic and radiative conditions (Qiu et al. 2023; Zhou et al. 2024). After bias correction, the ensemble mean of the two regional simulations is used to derive WBGT and associated heat-stress metrics.

2.4 Attribution methodology

To attribute the relative roles of T and q in driving WBGT changes, we employ a unified attribution framework composed of three complementary approaches. Each method targets a different aspect of variability: (1) long-term trends, (2) interannual fluctuations, and (3) differences in climatological means between historical and future climates. Although wind speed and radiation influence WBGT through the physical heat-balance model, they are not attributed explicitly here. This design isolates the dominant thermodynamic controls and enables a clearer interpretation of temperature versus moisture contributions.

(1) Trend decomposition: Long-term trends in *WBGTmax* (or *Nxday*) are attributed using a first-order linear decomposition based on the chain rule of calculus. This approach assumes that temporal changes in WBGTmax can be approximated as the linear sum of trends in its driving variables, weighted by their local sensitivities. At each grid point, the linear trend in WBGTmax is expressed as

$$\frac{d(WBGTmax)}{dt} \approx \beta_T \frac{dT}{dt} + \beta_q \frac{dq}{dt} + \varepsilon \quad (2)$$

https://doi.org/10.5194/egusphere-2026-829
Preprint. Discussion started: 4 March 2026

where $\frac{dX}{dt}$ denotes the linear trend (slope) of variable *X*, estimated using ordinary least squares (OLS) regression. The coefficients β_T and β_q represent the partial sensitivities of *WBGTmax* to *T* and *q*, respectively, obtained from a multiple linear regression of *WBGTmax* onto *T* and *q*. The term $\beta_T \frac{dT}{dt}$ and $\beta_q \frac{dq}{dt}$ quantify the contributions of temperature warming and atmospheric moistening (or drying), while ε represents the residual component not explained by linear *T*–*q* effects.

(2) Variability attribution: To quantify the relative importance of *T* and *q* in controlling interannual variability in *WBGTmax* (or *Nxday*), we employ Shapley value regression based on dominance analysis. This method evaluates the marginal contribution of each predictor to the model coefficient of determination (R^2) across all possible predictor combinations. The relative importance of a predictor x_k is defined as

$$I(x_k) = Average\left(R^2_{model\ with\ x_k} - R^2_{model\ without\ x_k}\right) \quad (3)$$

where the averaging is performed over all possible sub-model permutations. Based on these contributions, the total interannual variance of *WBGTmax* is approximately decomposed as

$$\sigma_{WBGTmax} \approx \sigma_T + \sigma_q + \sigma_{Unexplained} \quad (4)$$

where each term represents the fraction of interannual variance attributable to *T* variability, *q* variability, and unexplained processes, respectively. This approach explicitly quantifies the relative influence of thermodynamic drivers on year-to-year *WBGTmax* fluctuations, including those associated with large-scale climate variability such as ENSO.

(3) Mean-state change attribution: To attribute changes in the mean climatological state of *WBGTmax* (or *Nxday*) between the historical (1985–2014) and future (2071–2100) periods, we apply the Oaxaca–Blinder decomposition. This method partitions the change in mean WBGT into components explained by changes in the mean values of the driving variables and an unexplained (residual) term

https://doi.org/10.5194/egusphere-2026-829
Preprint. Discussion started: 4 March 2026

$$\Delta\overline{WBGTmax} = \overline{WBGTmax}_{fut} - \overline{WBGTmax}_{hist} \approx \beta_T\left(\overline{T}_{fut} - \overline{T}_{hist}\right) + \beta_q\left(\overline{q}_{fut} - \overline{q}_{hist}\right) + \varepsilon \quad (5)$$

where $\bar{X}_{\mathrm{hist}}$ and $\bar{X}_{\mathrm{fut}}$ denote the temporal means of variable X during the historical and future periods, respectively. The coefficients β_T and β_q are pooled regression coefficients derived from the combined historical and future datasets. The residual term ε captures contributions not explained by mean changes in T and q, including nonlinear responses and modifications of the WBGT–driver relationship.

3. Results

3.1 Drivers of historical (1985–2014) heat stress intensity

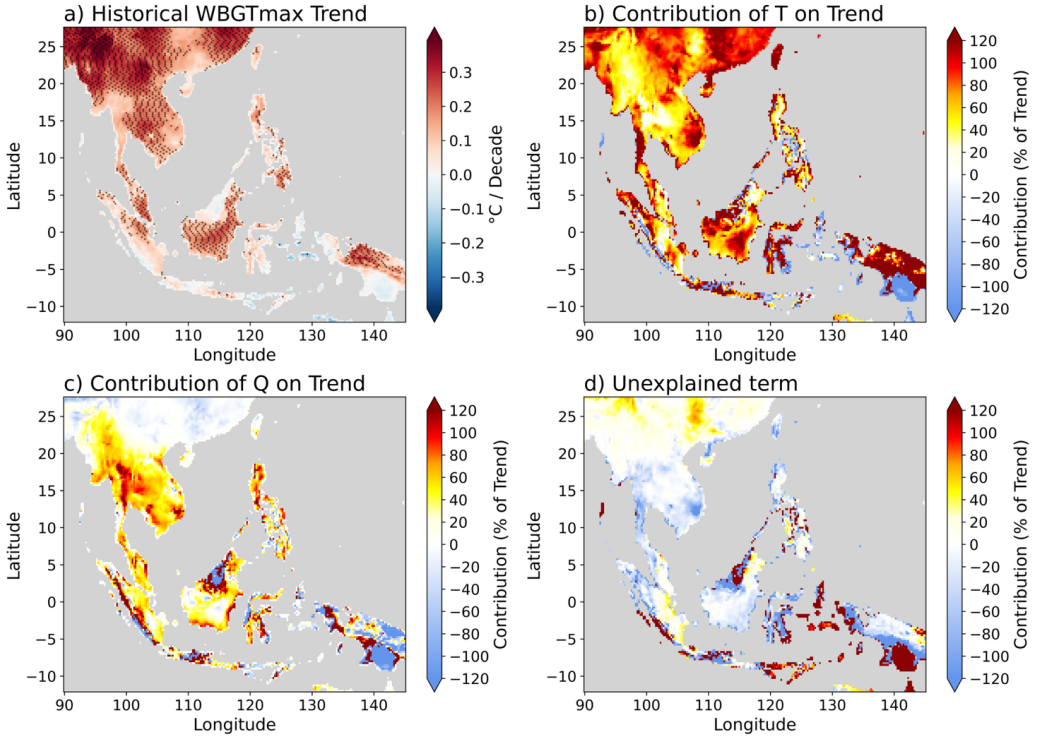

Figure 2: Spatial distribution of historical long-term trends in warm-season (April–October) daily maximum wet-bulb globe temperature (WBGTmax) over Southeast Asia during 1985–2014. (a) Linear trend in WBGTmax (°C decade⁻¹); stippling denotes statistical significance at $p < 0.05$. (b–d) Relative contributions

https://doi.org/10.5194/egusphere-2026-829
Preprint. Discussion started: 4 March 2026

(%) of near-surface air temperature (T), specific humidity (q), and the unexplained (residual) component to the WBGTmax trend.

Figure 2a displays the spatial distribution of linear trends in warm-season (April–October) daily maximum WBGT (*WBGTmax*) during the historical period (1985–2014). Positive trends occur across nearly all of SEA, indicating a widespread intensification of heat-stress conditions. Statistically significant increases of around 0.2 °C decade^{-1}, and locally higher, are concentrated over mainland Southeast Asia, the Malay Peninsula, parts of the eastern Philippines, and regions of the Maritime Continent such as Kalimantan and Papua. In contrast, weaker and more fragmented trends appear over some equatorial areas. Overall, the magnitude of the trends tends to increase toward higher latitudes and over elevated terrain, suggesting modulation by both geographic setting and topography.

The driver decomposition reveals pronounced spatial contrasts in the relative contributions of air temperature (T) and specific humidity (q) to historical *WBGTmax* trends (Figs. 2b–d). These patterns agree with the sub-regional synthesis (Fig. 4a) and with the corresponding trends in T and q (Fig. S1). A clear distinction emerges between monsoon-influenced regions of northern SEA (including lowland Indochina, the Philippines, and parts of Malay Peninsula) and the equatorial Maritime Continent. Over much of the equatorial Maritime Continent, *WBGTmax* trends are primarily controlled by T (Fig. 2b), indicating a predominantly temperature-controlled response to long-term warming. Elevated and mountainous regions, including northern Indochina (R18–R19), Myanmar (R20), Sulawesi (R06), and northern Papua (R08), also exhibit relatively weak contributions from q, suggesting limited amplification by atmospheric moistening. In contrast, substantial humidity-driven contributions are evident over the western Philippines (R01) and lowland monsoon regions of Mainland SEA, including southern Vietnam (R17), Cambodia (R16), southern Thailand (R15), and western Malaysia (R13) (Fig. 2c). These sub-regions stand out in Fig. 4a as exhibiting near-comparable contributions from T and q, highlighting the important amplifying role of atmospheric

https://doi.org/10.5194/egusphere-2026-829
Preprint. Discussion started: 4 March 2026

moistening. In these monsoon-affected environments, increasing q suppresses evaporative cooling and enhances *WBGTmax*, consistent with a moist-heat intensification mechanism. Comparable q-driven contributions are also found over northern Borneo (R03) and southern Papua (R09), although the associated trends are generally not statistically significant.

The unexplained (residual) component (Fig. 2d) is spatially heterogeneous but typically smaller than the thermodynamic terms and often negative, suggesting a modest damping relative to the combined thermodynamic effects of T and q.

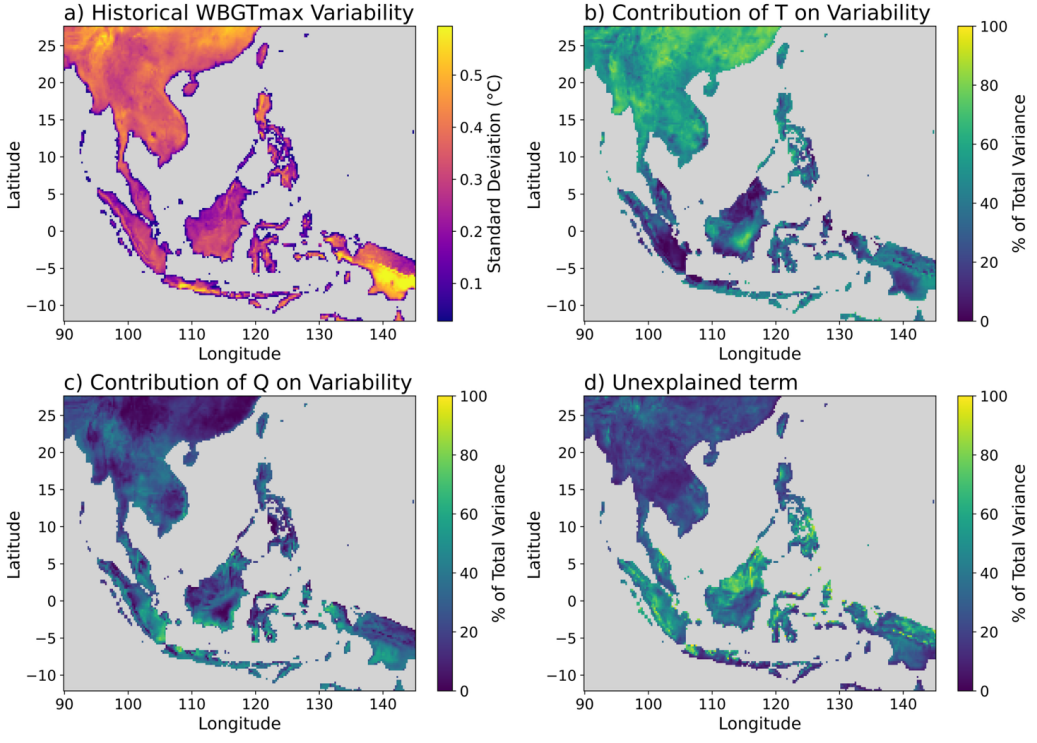

Figure 3: Spatial distribution of historical interannual variability in warm-season (April–October) daily maximum wet-bulb globe temperature (*WBGTmax*) over Southeast Asia during 1985–2014. (a) Interannual variability, quantified by its standard deviation, of *WBGTmax* (°C). (b–d) Relative contributions (%) of near-surface air temperature (T), specific humidity (q), and the unexplained (residual) component to the *WBGTmax* interannual variability.

https://doi.org/10.5194/egusphere-2026-829
Preprint. Discussion started: 4 March 2026

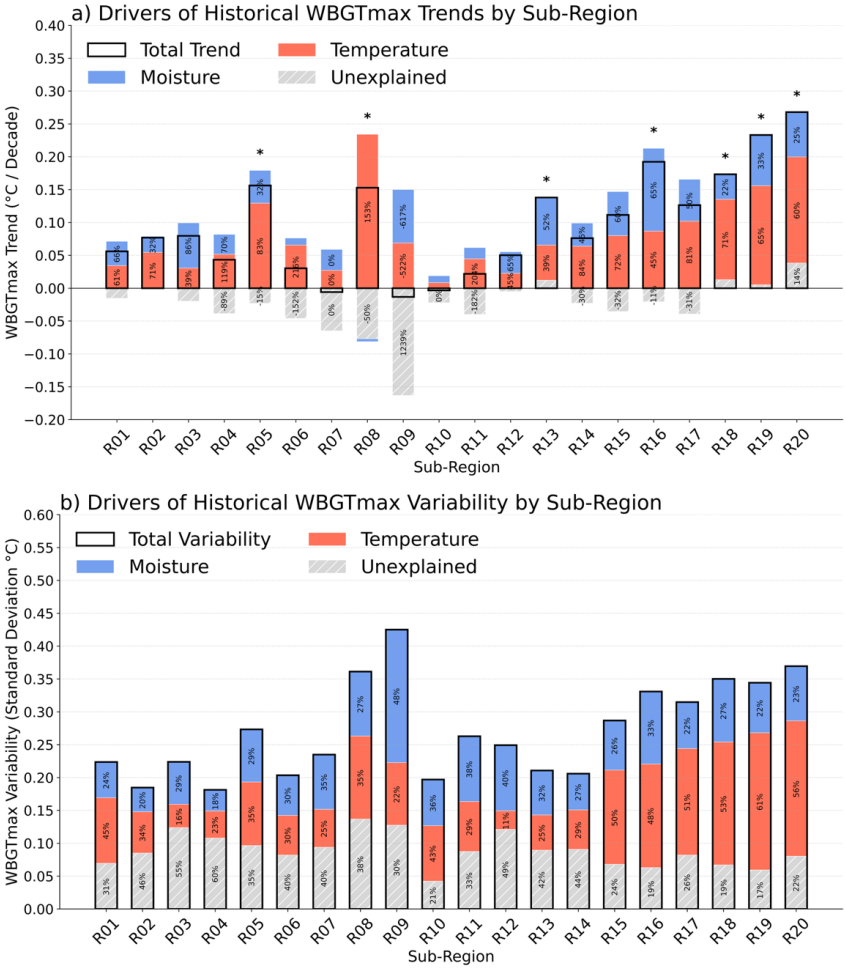

Figure 4: Area-averaged attribution of warm-season (April–October) *WBGTmax* historical trends and interannual variability across 20 Southeast Asia sub-regions (R01–R20) during 1985–2014. Black outlines indicate the total trends or variance. (a) Contributions of air temperature (*T*; red), specific humidity (*q*; blue), and the unexplained (hatched grey) term to sub-regional *WBGTmax* trends (°C decade^{-1}). Asterisks denote sub-regions with statistically significant trends at $p < 0.05$. (b) Fractional contributions (%) of *T*, *q*, and the unexplained term to total *WBGTmax* interannual variance (°C).

Figure 3a presents the interannual variability of *WBGTmax*, quantified by its standard deviation, during 1985–2014. Larger variability of about 0.3–0.4 °C or even higher is found over much of Mainland SEA and parts of the Maritime Continent, with pronounced maxima over northern Indochina and easternmost Indonesia in the Southern Hemisphere. In contrast, equatorial oceanic

https://doi.org/10.5194/egusphere-2026-829
Preprint. Discussion started: 4 March 2026

regions and the southern Philippines display weaker fluctuations, generally below 0.3 °C, consistent with strong ocean–atmosphere coupling and muted year-to-year temperature fluctuations. This pattern indicates greater sensitivity of continental and highland areas to year-to-year climate variations compared with maritime environments.

The attribution of interannual *WBGTmax* variability (Figs. 3b–d), together with the corresponding variability in *T* and *q* (Fig. S2), shows a clear though not absolute mainland–maritime contrast. Over areas north of aproximately 10°N including Mainland SEA and northern Philippines, variability in *T* explains a large fraction of *WBGTmax* variability (Fig. 3b). This reflects a temperature-limited regime in which year-to-year variations in large-scale circulation, monsoon strength, and episodic cold-air intrusions efficiently translate into WBGT anomalies. In contrast, across much of the Maritime Continent (R05–R12), including Sumatra, Borneo, and western Indonesia, *q* becomes an important, though not dominant, contributor (Fig. 3c). In these persistently warm environments, relatively weak internannual variability in *T* allows fluctuations in *q* associated with circulation anomalies associated with ENSO and the Madden–Julian Oscillation to exert a strong influence on heat-stress variability.

Notably, the unexplained (residual) component (Fig. 3d) accounts for a substantial fraction of total interannual variance over large parts of SEA, particularly over the eastern Philippines (R02) and much of the Maritime Continent (R03–R14). In many sub-regions, the unexplained component equals or exceeds the individual *T* or *q* contributions. This indicates that nonlinear temperature–humidity interactions and compound anomalies play a major role in shaping interannual extreme heat stress, beyond what is captured by a linear additive framework. Together, these patterns identify two distinct variability regimes: a temperature-controlled regime over monsoon-influenced continental regions, and an interaction-dominated regime over the Maritime Continent, where persistently high background humidity makes *WBGTmax* variability highly sensitive to compound thermodynamic anomalies rather than to variability in a single driver. The regional summary (Fig. 4b) highlights

https://doi.org/10.5194/egusphere-2026-829
Preprint. Discussion started: 4 March 2026

these regimes. This shows that while *T* dominates variability in Mainland SEA sub-regions, Maritime Continent regions exhibit a more even partitioning among *T*, *q*, and the unexplained component, with the latter exceeding 40% in several sub-regions (e.g., R03–R04, R12–R14).

Comparing this with the trend attribution reveals an important contrast: long-term trends in *WBGTmax* reflect relatively smooth, additive thermodynamic forcing, whereas interannual variability arises primarily from episodic compounding of temperature and moisture anomalies.

3.2 Drivers of historical (1985–2014) heat stress frequency

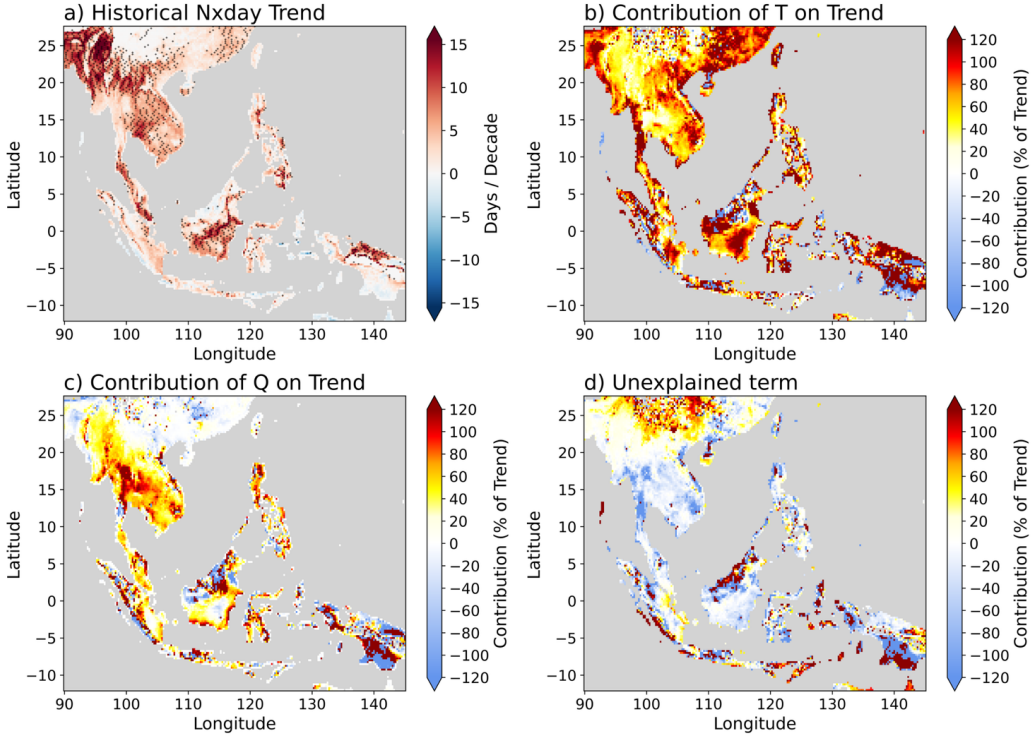

Figure 5: Spatial distribution of historical long-term trends in warm-season (April–October) annual number of extreme heat-stress days (*Nxday*) over Southeast Asia during 1985–2014. (a) Linear trend in *Nxday* (days decade^{-1}); stippling denotes statistical significance at $p < 0.05$. (b–d) Relative contributions (%) of air temperature (*T*), specific humidity (*q*), and the unexplained (residual) component to *Nxday* trends.

https://doi.org/10.5194/egusphere-2026-829
Preprint. Discussion started: 4 March 2026

Building on the analysis of *WBGTmax* intensity, we next assess changes in the frequency of extreme heat stress using *Nxday*. The spatial distribution and dominant controls closely resemble those identified for *WBGTmax*, indicating common thermodynamic drivers. During the historical period (1985–2014), *Nxday* exhibits widespread increasing trends across SEA (Fig. 5a). Statistically significant trends are concentrated over mainland regions, western Malaysia, and parts of the Maritime Continent. In several locations, particularly northwestern Indochina and high-elevation areas, increases reach roughly 8–10 days decade^{-1}, indicating a rapid rise in the occurrence of extreme heat-stress conditions.

The decomposition points to a dominant, though not exclusive, role of T (Fig. 5b). Over large parts of the domain, warming explains most of the increase in threshold exceedances, reflecting the strong sensitivity of *Nxday* to shifts in the background climate. Moisture contributions (Fig. 5c) are more evident in monsoon-influenced lowlands, where higher humidity raises baseline WBGT and increases the probability of surpassing the threshold, consistent with the behavior found for *WBGTmax*. In contrast, many Maritime Continent regions display weaker and less coherent contributions from q, consistent with smaller mean changes and stronger modulation by variability. The unexplained (residual) component (Fig. 5d) is spatially heterogeneous and generally negative for long-term trends, implying a modest damping of the combined thermodynamic effect.

The sub-regional synthesis (Fig. 5a) corroborates this picture. Northern Mainland SEA sub-regions (R18–R20) show robust, temperature-dominated increases in Nxday, while q plays a secondary but visible role in lowland monsoon regions such as R13 and R15–R17, and in several maritime regions (e.g., R05 and R07). Overall, maritime areas exhibit smaller and less consistently significant trends, consistent with weaker warming and stronger modulation by moisture variability.

Interannual variability in *Nxday* (Fig. 6a) is substantial, often exceeding 10 days over both Mainland SEA and Maritime Continent. Compared with *WBGTmax*, however, the attribution reveals a stronger dominance of the unexplained component in variability in *Nxday*. Although variations in T

https://doi.org/10.5194/egusphere-2026-829
Preprint. Discussion started: 4 March 2026

and q contribute locally (Figs. 6b–c), neither variable alone accounts for most of the variance across large portions of SEA. Instead, the unexplained term (Fig. 6d) explains a major share of the total variability, indicating an essential role for nonlinear threshold behavior and compound anomalies.

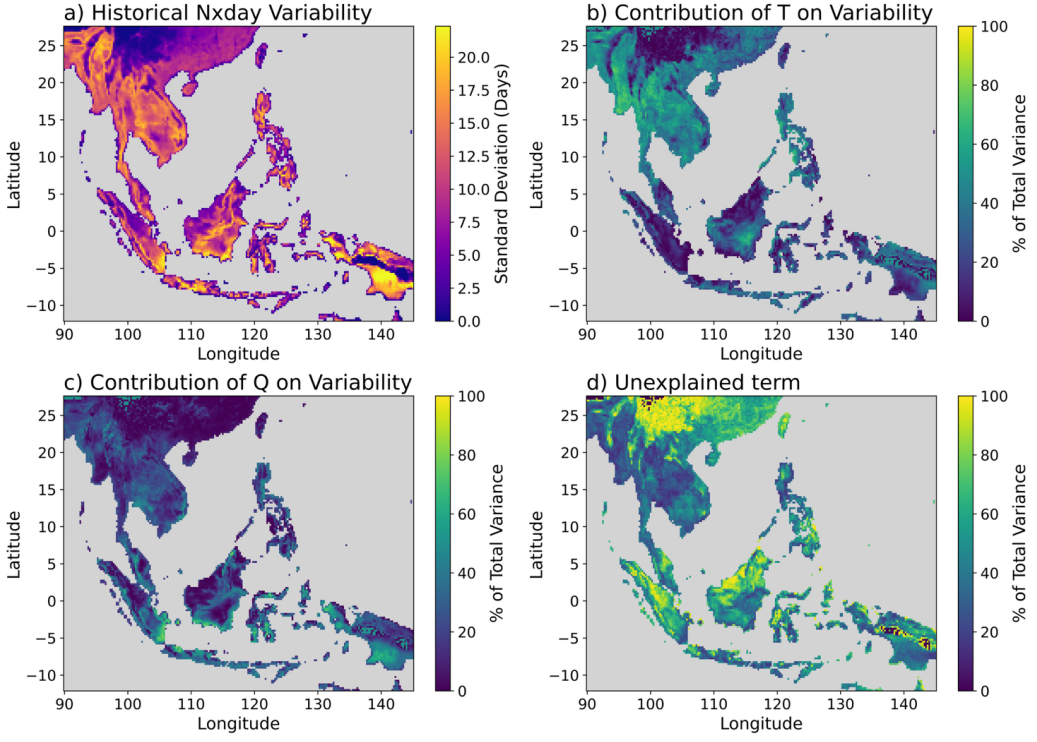

Figure 6: Spatial distribution of historical interannual variability in warm-season (April–October) annual number of extreme heat-stress days (*Nxday*) over Southeast Asia during 1985–2014. (a) (a) Interannual variability, quantified by its standard deviation, of *Nxday* (days). (b–d) Relative contributions (%) of near-surface air temperature (T), specific humidity (q), and the unexplained (residual) component to the *Nxday* interannual variability.

The physical interpretation of this residual differs by region. In monsoon-dominated areas, year-to-year, year-to-year variability in *Nxday* often reflects episodic warm and humid seasons that shift a large part of the distribution above the critical threshold. Meanwhile, over the Maritime Continent, where background humidity is persistently high, relatively small concurrent changes in T–q can produce disproportionately large changes in exceedance frequency. This regime dependence is

https://doi.org/10.5194/egusphere-2026-829
Preprint. Discussion started: 4 March 2026

confirmed by the sub-regional synthesis (Fig. 7b), in which the unexplained component typically accounts for 40–60% of total *Nxday* variability. The result underscores that compound thermodynamic anomalies, rather than fluctuations in a single driver, govern much of the variability in extreme heat-stress frequency.

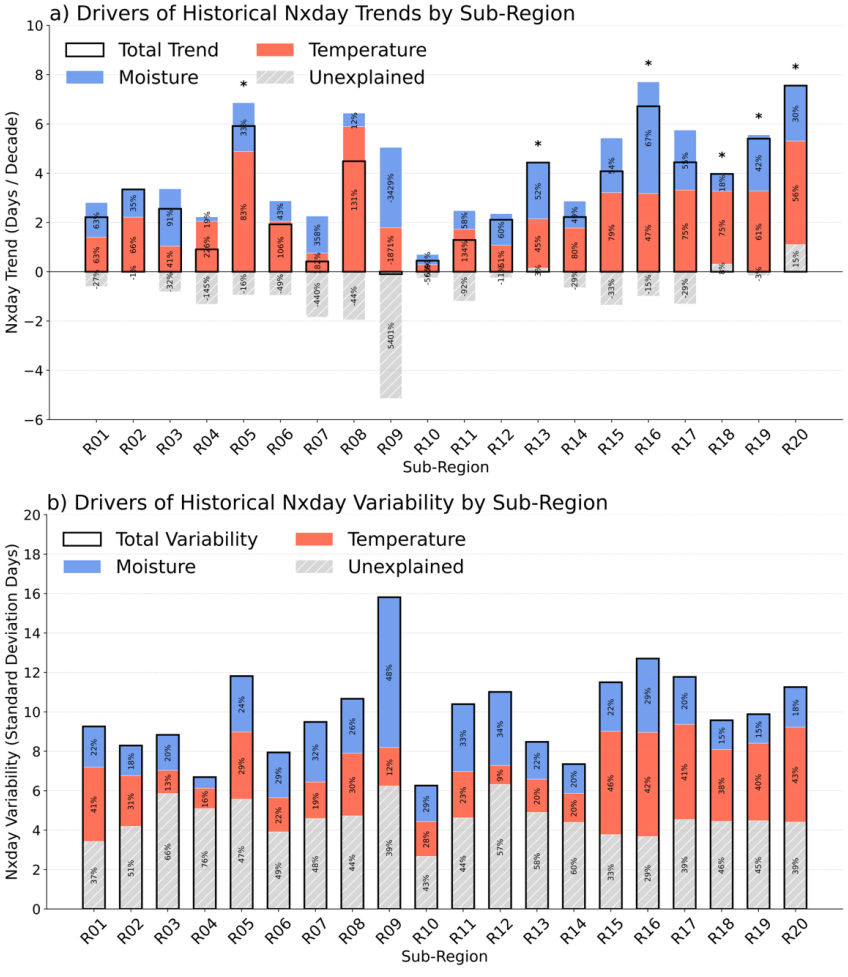

Figure 7: Area-averaged attribution of warm-season (April–October) *Nxday* historical trends and interannual variability across 20 Southeast Asia sub-regions (R01–R20) during 1985–2014. Black outlines indicate the total trends or variance. (a) Contributions of air temperature (T; red), specific humidity (q; blue), and the unexplained (residual; hatched grey) term to sub-regional *Nxday* trends (days decade^{-1}). Asterisks denote sub-regions with statistically significant trends at $p < 0.05$. (b) Fractional contributions (%) of T, q, and the unexplained component to total *Nxday* interannual variance (days).

https://doi.org/10.5194/egusphere-2026-829
Preprint. Discussion started: 4 March 2026

3.2 Drivers of future (2071–2100) minus (1985–2014) changes

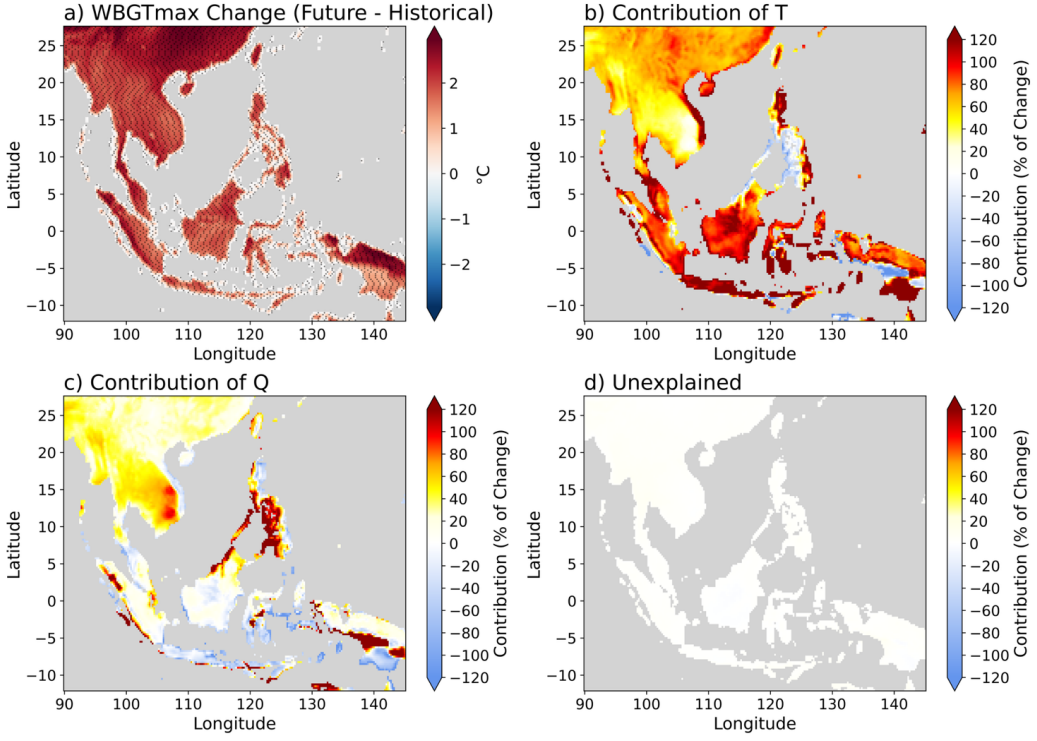

Figure 8: Spatial patterns of projected changes in warm-season (April–October) daily maximum wet-bulb globe temperature (*WBGTmax*) over Southeast Asia between the historical (1985–2014) and the future (2071–2100) periods under the SSP5-8.5 scenario. (a) The total change (future minus historical periods); stippling denotes statistical significance at $p < 0.05$. (b), (c) and (d) Relative contributions (%) of air temperature (*T*), specific humidity (*q*) and unexplained (residual) component, respectively, to projected *WBGTmax* changes.

Future projections under SSP5–8.5, relative to the historical climatology (Figs. S3 and S4), show large and spatially coherent increases in warm-season *WBGTmax* across SEA (Fig. 8a). Regional-mean increases typically exceed approximately 1.5–2 °C and are locally higher over mainland areas and parts of the eastern Maritime Continent. The widespread and spatially consistent nature of the projected warming indicates a basin-scale upward shift in the *WBGTmax* distribution, rather than localized or region-specific intensification. This coherence points to large-scale thermodynamic forcing as the primary driver of future heat-stress intensification.

https://doi.org/10.5194/egusphere-2026-829
Preprint. Discussion started: 4 March 2026

The attribution indicates that *T* remains the dominant driver to future increases in *WBGTmax*, particularly over the Maritime Continent (Fig. 8b). However, unlike the historical period, *q* now contributes positively and often substantially throughout the region (Fig. 8c). Over monsoon-influenced regions, including the Philippines and lowland Mainland SEA, the contribution from *q* frequently accounts for approximately 30–50% of the projected WBGTmax increase. This widespread amplification reflects concurrent warming and moistening expected in a warmer climate and signals a transition toward more compound warm–humid conditions, consistent with Clausius–Clapeyron scaling and projected increases in both *T* and *q* under SSP5–8.5 (Fig. S5).

The unexplained (residual) contribution is negligible over most areas (Fig. 8d), indicating that future *WBGTmax* changes well explained by first-order thermodynamic adjustments. The sub-regional synthesis (Fig. 10a) reinforces this finding: All sub-regions exhibiting statistically significant increases in *WBGTmax*, with *T* dominating across most Maritime Continent sub-regions (R03–R14), while monsoon-influenced sub-regions of Mainland SEA and the Philippines (R01–R02, R15–R20) show more comparable roles from *T* and *q*. Together, these results highlight a growing control of moist enthalpy on future heat stress, rather than dry-bulb warming alone.

The frequency of extreme heat stress *Nxday* also increases dramatically by the end of the century under SSP5–8.5 (Fig. 9a) compared with the historical climatology (Figs. S3 and S4). Many regions experience rises of several tens of days per year, with some mainland and maritime locations exceeding ~50–60 days year^{-1}. The strong spatial similarity with *WBGTmax* changes indicates that higher background heat stress translates directly into more frequent threshold exceedances.

Temperature again provides the dominant contribution (Fig. 9b). Compared with *WBGTmax*, the contribution from *q* is systematically weaker (Fig. 9c). While background moistening elevates baseline WBGT, the frequency of threshold exceedance is primarily governed by shifts in mean *T* relative to a fixed extreme heat-stress threshold. The unexplained (residual) term remains minimal

https://doi.org/10.5194/egusphere-2026-829
Preprint. Discussion started: 4 March 2026

(Fig. 9d), underscoring that projected *Nxday* changes are largely governed by straightforward thermodynamic forcing.

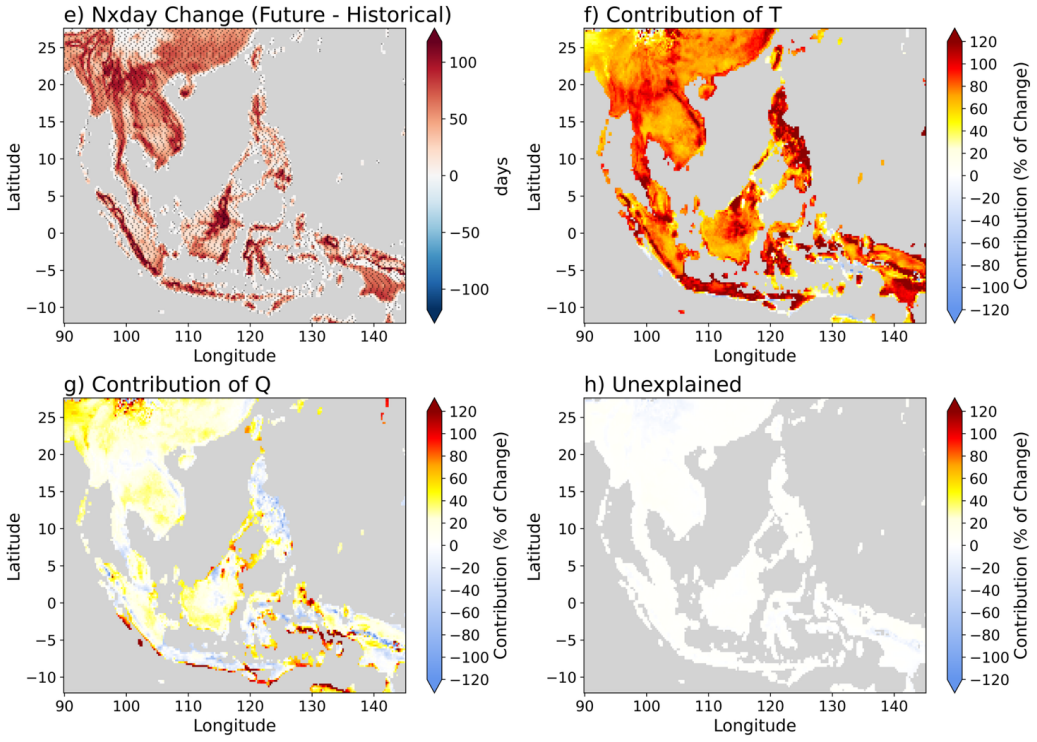

Figure 9: Spatial patterns of projected changes in warm-season (April–October) annual number of extreme heat-stress days (*Nxday*) over Southeast Asia between the historical (1985–2014) and the future (2071–2100) periods under the SSP5-8.5 scenario. (a) The total change (future minus historical periods); stippling denotes statistical significance at $p < 0.05$. (b), (c) and (d) Relative contributions (%) of air temperature (*T*), specific humidity (*q*) and unexplained (residual) component, respectively, to projected *Nxday* changes.

Despite broadly similar spatial patterns, *Nxday* exhibits a stronger amplification of future changes than *WBGTmax* owing to its nonlinear response to mean-state warming. Even modest increases in mean WBGT can produce large rises in in the number of exceedance days, particularly in regions already close to critical heat-stress thresholds. This sensitivity is confirmed in the sub-regional synthesis (Fig. 10b), where *T* explains approximately 70–90% of projected *Nxday* increases,

https://doi.org/10.5194/egusphere-2026-829
Preprint. Discussion started: 4 March 2026

while *q* provides a secondary but regionally important enhancement, particularly in monsoon-influenced and coastal environments.

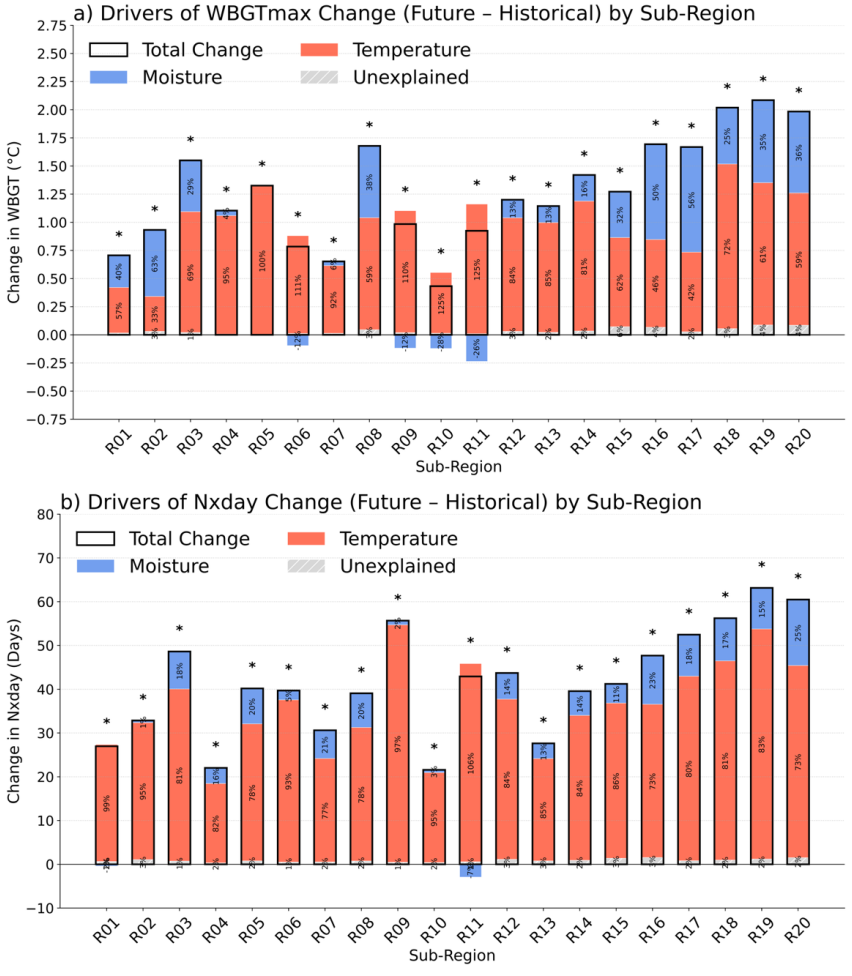

Figure 10: Area-averaged attribution of future minus historical changes in warm-season (April–October) (a) *WBGTmax* and (b) *Nxday* across 20 Southeast Asia sub-regions (R01–R20). Black outlines indicate the total change between 1985–2014 and 2071–2100. Colored bars represent contributions from temperature (*T*; red), specific humidity (*q*; blue), and the unexplained component (hatched grey). Asterisks denote sub-regions with statistically significant total changes at $p < 0.05$.

https://doi.org/10.5194/egusphere-2026-829
Preprint. Discussion started: 4 March 2026

4. Discussions and Conclusions

This study presents a unified thermodynamic attribution of warm-season (April–October) heat stress across Southeast Asia (SEA) by separating the contributions of near-surface air temperature (T), specific humidity (q), and non-linear unexplained (residual) processes across multiple timescales.

During the historical period (1985–2014), increases in both heat-stress intensity (*WBGTmax*) and frequency (*Nxday*) are driven primarily by rising T, particularly over the Maritime Continent and elevated terrain. Nevertheless, q already exerts an important amplifying influence in monsoon-affected lowlands, including Indochina, the Philippines, and parts of the Malay Peninsula. These results demonstrate that contemporary heat stress in SEA cannot be understood from temperature change alone.

Future projections (2071–2100) under SSP5-8.5 reveal a systematic strengthening of compound warm–humid conditions by the end of the 21st century. Although T remains the leading contributor to projected increases in both *WBGTmax* and *Nxday*, q becomes uniformly positive and often comparable in magnitude, especially in monsoon-influenced regions. This response is consistent with thermodynamic expectations of enhanced atmospheric water-holding capacity in a warmer climate and implies a continued decline in evaporative cooling efficiency. Consequently, late-century heat stress is increasingly governed by elevated moist enthalpy rather than dry-bulb warming alone.

A further distinction arises between long-term trends and interannual variability. Historical trends and future mean-state shifts explained by relatively smooth thermodynamic adjustments, whereas year-to-year variability, particularly over the Maritime Continent, is strongly shaped by non-linear interactions between T and q. This behavior is most pronounced for exceedance-based metrics such as *Nxday*, where small co-occurring anomalies can trigger large changes in frequency. Hence, while gradual warming provides a predictable background intensification, seasonal extremes remain

https://doi.org/10.5194/egusphere-2026-829
Preprint. Discussion started: 4 March 2026

strongly influenced by compound processes whose importance varies between continental monsoon and maritime regimes.

The projected intensification of extreme heat stress has important implications for hazard management and adaptation across SEA. More frequent exceedances of extreme WBGT thresholds point to increasing risks for outdoor labor and vulnerable populations, particularly in regions with high population density and limited adaptive capacity. Traditional protective measures such as rest scheduling, hydration, and workload modification will remain necessary but may become less effective as humidity rises (Morabito et al., 2019). Early-warning systems and risk frameworks that incorporate both T and q are therefore likely to outperform approaches based solely on T. At the same time, expanding demand for mechanical cooling raises challenges for energy infrastructure and emissions, emphasizing the need for coordinated strategies linking climate risk, urban planning, and public health.

Several limitations warrant consideration. This study does not explicitly quantify labor productivity losses or economic impacts, which are known to be highly sensitive to WBGT threshold exceedances. In addition, urban heat-island (UHI) effects are not resolved at the sub-regional scale and may further amplify heat stress in major metropolitan areas. The projections also assume limited adaptation and should therefore be interpreted as upper-bound estimates under the assumed emissions scenario (Russo et al. 2019). Finally, while wind and radiation are included within WBGT calculations, their individual contributions are not separately attributed, and evolving circulation variability could further shape future extremes. Addressing these issues represents a priority for future work.

Supplementary Information The manuscript contains supplementary figures

Acknowledgments This study is conducted as part of the Vietnam Academy of Science and Technology (VAST) under Grant THTETN.01/25-26. The downscaled CMIP6 data were obtained from the SEACLID/CORDEX-SEA project funded by the Asia Pacific Network for Global Change

https://doi.org/10.5194/egusphere-2026-829
Preprint. Discussion started: 4 March 2026

Research (CRRP2023-658 08MY-Cruz) and by the Vietnam National Foundation for Science and Technology Development (NAFOSTED) under Grant 105.06-2021.14.

Funding This study is funded by VAST under Grant THTETN.01/25-26.

Data Availability Outputs from CMIP6 global climate models are accessed via https://esgf-node.ipsl.upmc.fr/projects/cmip6-ipsl/, while the ECMWF ERA5 was downloaded from https://www.ecmwf.int/en/forecasts/dataset/ecmwf-reanalysis-v5. The RegCM downscaling outputs and the WBGT datasets generated in this study are available from the corresponding author upon reasonable request.

Code availability Codes used in this study are available upon reasonable requests from the corresponding author.

Author contributions The author conceived the study, performed the analysis, and wrote the manuscript.

Declarations

Conflict of interest The authors declare no competing interests.

Ethical approval Ethical approval is not applicable to this article.

References

Anon: Prevention of thermal injuries during distance running: Position stand, Medical Journal of Australia, 141, 876–879, https://doi.org/10.5694/j.1326-5377.1984.tb132981.x, 1984.

Barriopedro, D., Fischer, E. M., Luterbacher, J., Trigo, R. M., and García-Herrera, R.: The Hot Summer of 2010: Redrawing the Temperature Record Map of Europe, Science, 332, 220–224, https://doi.org/10.1126/science.1201224, 2011.

https://doi.org/10.5194/egusphere-2026-829
Preprint. Discussion started: 4 March 2026

Buzan, J. R. and Huber, M.: Moist Heat Stress on a Hotter Earth, Annu. Rev. Earth Planet. Sci., 48, 623–655, https://doi.org/10.1146/annurev-earth-053018-060100, 2020.

Chang, C.-P., Wang, Z., McBride, J., and Liu, C.-H.: Annual Cycle of Southeast Asia—Maritime Continent Rainfall and the Asymmetric Monsoon Transition, Journal of Climate, 18, 287–301, https://doi.org/10.1175/JCLI-3257.1, 2005.

Coppola, E., Stocchi, P., Pichelli, E., Torres Alavez, J. A., Glazer, R., Giuliani, G., Di Sante, F., Nogherotto, R., and Giorgi, F.: Non-Hydrostatic RegCM4 (RegCM4-NH): model description and case studies over multiple domains, Geosci. Model Dev., 14, 7705–7723, https://doi.org/10.5194/gmd-14-7705-2021, 2021.

Cruz, F. T., Narisma, G. T., Dado, J. B., Singhruck, P., Tangang, F., Linarka, U. A., Wati, T., Juneng, L., Phan-Van, T., Ngo-Duc, T., Santisirisomboon, J., Gunawan, D., and Aldrian, E.: Sensitivity of temperature to physical parameterization schemes of RegCM4 over the CORDEX - Southeast Asia region, Intl Journal of Climatology, 37, 5139–5153, https://doi.org/10.1002/joc.5151, 2017.

Douville, H., Qasmi, S., Ribes, A., and Bock, O.: Global warming at near-constant tropospheric relative humidity is supported by observations, Commun Earth Environ, 3, 237, https://doi.org/10.1038/s43247-022-00561-z, 2022.

Dunne, J. P., Stouffer, R. J., and John, J. G.: Reductions in labour capacity from heat stress under climate warming, Nature Clim Change, 3, 563–566, https://doi.org/10.1038/nclimate1827, 2013.

Earth Resources Observation and Science (EROS) Center: Global 30 Arc-Second Elevation (GTOPO30), https://doi.org/10.5066/F7DF6PQS, 2017.

https://doi.org/10.5194/egusphere-2026-829
Preprint. Discussion started: 4 March 2026

Eyring, V., Bony, S., Meehl, G. A., Senior, C. A., Stevens, B., Stouffer, R. J., and Taylor, K. E.: Overview of the Coupled Model Intercomparison Project Phase 6 (CMIP6) experimental design and organization, Geosci. Model Dev., 9, 1937–1958, https://doi.org/10.5194/gmd-9-1937-2016, 2016.

Hersbach, H., Bell, B., Berrisford, P., Hirahara, S., Horányi, A., Muñoz-Sabater, J., Nicolas, J., Peubey, C., Radu, R., Schepers, D., Simmons, A., Soci, C., Abdalla, S., Abellan, X., Balsamo, G., Bechtold, P., Biavati, G., Bidlot, J., Bonavita, M., De Chiara, G., Dahlgren, P., Dee, D., Diamantakis, M., Dragani, R., Flemming, J., Forbes, R., Fuentes, M., Geer, A., Haimberger, L., Healy, S., Hogan, R. J., Hólm, E., Janisková, M., Keeley, S., Laloyaux, P., Lopez, P., Lupu, C., Radnoti, G., De Rosnay, P., Rozum, I., Vamborg, F., Villaume, S., and Thépaut, J.: The ERA5 global reanalysis, Quart J Royal Meteoro Soc, 146, 1999–2049, https://doi.org/10.1002/qj.3803, 2020.

Im, E.-S., Pal, J. S., and Eltahir, E. A. B.: Deadly heat waves projected in the densely populated agricultural regions of South Asia, Sci. Adv., 3, e1603322, https://doi.org/10.1126/sciadv.1603322, 2017.

ISO: Ergonomics of the thermal environment. Assessment of heat stress using the WBGT (wet bulb globe temperature) index, 26 pp., 2017.

Juneng, L., Tangang, F., Chung, J., Ngai, S., Tay, T., Narisma, G., Cruz, F., Phan-Van, T., Ngo-Duc, T., Santisirisomboon, J., Singhruck, P., Gunawan, D., and Aldrian, E.: Sensitivity of Southeast Asia rainfall simulations to cumulus and air-sea flux parameterizations in RegCM4, Clim. Res., 69, 59–77, https://doi.org/10.3354/cr01386, 2016.

Kjellstrom, T., Briggs, D., Freyberg, C., Lemke, B., Otto, M., and Hyatt, O.: Heat, Human Performance, and Occupational Health: A Key Issue for the Assessment of Global Climate Change Impacts, Annu. Rev. Public Health, 37, 97–112, https://doi.org/10.1146/annurev-publhealth-032315-021740, 2016.

https://doi.org/10.5194/egusphere-2026-829
Preprint. Discussion started: 4 March 2026

Kjellstrom, T., Freyberg, C., Lemke, B., Otto, M., and Briggs, D.: Estimating population heat exposure and impacts on working people in conjunction with climate change, Int J Biometeorol, 62, 291–306, https://doi.org/10.1007/s00484-017-1407-0, 2018.

Kong, Q. and Huber, M.: Explicit Calculations of Wet-Bulb Globe Temperature Compared With Approximations and Why It Matters for Labor Productivity, Earth's Future, 10, e2021EF002334, https://doi.org/10.1029/2021EF002334, 2022.

Kushwaha, R., Kumar, P., and Hisaki, Y.: Global future heat stress projections: Regional variations of Humidex changes from high-resolution CMIP6 models, Atmospheric Research, 327, 108367, https://doi.org/10.1016/j.atmosres.2025.108367, 2026.

Lee, S.-M. and Min, S.-K.: Heat Stress Changes over East Asia under 1.5° and 2.0°C Global Warming Targets, J. Climate, 31, 2819–2831, https://doi.org/10.1175/JCLI-D-17-0449.1, 2018.

Liljegren, J. C., Carhart, R. A., Lawday, P., Tschopp, S., and Sharp, R.: Modeling the Wet Bulb Globe Temperature Using Standard Meteorological Measurements, Journal of Occupational and Environmental Hygiene, 5, 645–655, https://doi.org/10.1080/15459620802310770, 2008.

Manimaran, S., Wagenaar, D., Nam, C., Kasmalkar, I., Lierhammer, L., Bouwer, L. M., and Lallemant, D.: Widespread heat stress will become the norm in a warming Southeast Asia, Sci Rep, 15, 45799, https://doi.org/10.1038/s41598-025-28817-6, 2025.

Matsumoto, J.: Seasonal transition of summer rainy season over indochina and adjacent monsoon region, Adv. Atmos. Sci., 14, 231–245, https://doi.org/10.1007/s00376-997-0022-0, 1997.

Matthews, T. K. R., Wilby, R. L., and Murphy, C.: Communicating the deadly consequences of global warming for human heat stress, Proc. Natl. Acad. Sci. U.S.A., 114, 3861–3866, https://doi.org/10.1073/pnas.1617526114, 2017.

https://doi.org/10.5194/egusphere-2026-829
Preprint. Discussion started: 4 March 2026

548 Mohammad, P. and Weng, Q.: Asian heat stress variations in a changing climate: Implications for
549 disproportionate urban and rural population exposure, Habitat International, 156, 103294,
550 https://doi.org/10.1016/j.habitatint.2025.103294, 2025.

551 Morabito, M., Messeri, A., Noti, P., Casanueva, A., Crisci, A., Kotlarski, S., Orlandini, S., Schwierz,
552 C., Spirig, C., Kingma, B. R. M., Flouris, A. D., and Nybo, L.: An Occupational Heat–Health
553 Warning System for Europe: The HEAT-SHIELD Platform, IJERPH, 16, 2890,
554 https://doi.org/10.3390/ijerph16162890, 2019.

555 Ngo-Duc, T., Nguyen-Duy, T., Desmet, Q., Trinh-Tuan, L., Ramu, L., Cruz, F., Dado, J. M., Chung,
556 J. X., Phan-Van, T., Pham-Thanh, H., Truong-Ba, K., Tangang, F. T., Juneng, L., Santisirisomboon,
557 J., Srisawadwong, R., Permana, D., Linarka, U. A., and Gunawan, D.: Performance ranking of
558 multiple CORDEX-SEA sensitivity experiments: towards an optimum choice of physical schemes
559 for RegCM over Southeast Asia, Clim Dyn, 62, 8659–8673, https://doi.org/10.1007/s00382-024-
560 07353-5, 2024.

561 Nguyen-Le, D.: Climatology of the global summer monsoon rainy seasons: Revisited from a high-
562 resolution satellite climate data record, Atmospheric Research, 289, 106749,
563 https://doi.org/10.1016/j.atmosres.2023.106749, 2023.

564 Nguyen–Le, D.: Projected ENSO teleconnection on the Southeast Asian climate under global
565 warming, Environ. Res. Lett., 19, 014001, https://doi.org/10.1088/1748-9326/ad0d3e, 2024.

566 Nguyen-Le, D., Nguyen-Xuan, T., Nguyen-Duy, T., Trinh-Tuan, L., and Ngo-Duc, T.: Assessment
567 of future heat stress in Vietnam using physically based wet-bulb globe temperature and high-
568 resolution downscaled projections, Environ. Res. Commun., 8, 015017,
569 https://doi.org/10.1088/2515-7620/ae3897, 2026.

570 O'Neill, B. C., Kriegler, E., Ebi, K. L., Kemp-Benedict, E., Riahi, K., Rothman, D. S., Van Ruijven,
571 B. J., Van Vuuren, D. P., Birkmann, J., Kok, K., Levy, M., and Solecki, W.: The roads ahead:

https://doi.org/10.5194/egusphere-2026-829
Preprint. Discussion started: 4 March 2026

572 Narratives for shared socioeconomic pathways describing world futures in the 21st century, Global
573 Environmental Change, 42, 169–180, https://doi.org/10.1016/j.gloenvcha.2015.01.004, 2017.

574 Overland, I., Sagbakken, H. F., Chan, H.-Y., Merdekawati, M., Suryadi, B., Utama, N. A., and
575 Vakulchuk, R.: The ASEAN climate and energy paradox, Energy and Climate Change, 2, 100019,
576 https://doi.org/10.1016/j.egycc.2020.100019, 2021.

577 Qiu, L., Zhu, Z., Zhou, Z., Im, E.-S., Min, S.-K., Kim, Y.-H., Kim, Y., Cha, D.-H., Ahn, J.-B., and
578 Byun, Y.-H.: Amplification of the discrepancy between simplified and physics-based wet-bulb globe
579 temperatures in a warmer climate, Weather and Climate Extremes, 44, 100677,
580 https://doi.org/10.1016/j.wace.2024.100677, 2024.

581 Räsänen, T. A., Lindgren, V., Guillaume, J. H. A., Buckley, B. M., and Kummu, M.: On the spatial
582 and temporal variability of ENSO precipitation and drought teleconnection in mainland Southeast
583 Asia, Climate of the Past, 12, 1889–1905, https://doi.org/10.5194/cp-12-1889-2016, 2016.

584 Raymond, C., Matthews, T., and Horton, R. M.: The emergence of heat and humidity too severe for
585 human tolerance, Sci. Adv., 6, eaaw1838, https://doi.org/10.1126/sciadv.aaw1838, 2020.

586 Russo, S., Sillmann, J., Sippel, S., Barcikowska, M. J., Ghisetti, C., Smid, M., and O'Neill, B.: Half
587 a degree and rapid socioeconomic development matter for heatwave risk, Nat Commun, 10, 136,
588 https://doi.org/10.1038/s41467-018-08070-4, 2019.

589 Schwingshackl, C., Sillmann, J., Vicedo-Cabrera, A. M., Sandstad, M., and Aunan, K.: Heat Stress
590 Indicators in CMIP6: Estimating Future Trends and Exceedances of Impact-Relevant Thresholds,
591 Earth's Future, 9, e2020EF001885, https://doi.org/10.1029/2020EF001885, 2021.

592 Tangang, F., Chung, J. X., Juneng, L., Supari, Salimun, E., Ngai, S. T., Jamaluddin, A. F., Mohd, M.
593 S. F., Cruz, F., Narisma, G., Santisirisomboon, J., Ngo-Duc, T., Van Tan, P., Singhruck, P.,
594 Gunawan, D., Aldrian, E., Sopaheluwakan, A., Grigory, N., Remedio, A. R. C., Sein, D. V., Hein-

https://doi.org/10.5194/egusphere-2026-829
Preprint. Discussion started: 4 March 2026

595 Griggs, D., McGregor, J. L., Yang, H., Sasaki, H., and Kumar, P.: Projected future changes in
596 rainfall in Southeast Asia based on CORDEX–SEA multi-model simulations, Clim Dyn, 55, 1247–
597 1267, https://doi.org/10.1007/s00382-020-05322-2, 2020.

598 Wang, B. and LinHo: Rainy Season of the Asian–Pacific Summer Monsoon*, J. Climate, 15, 386–
599 398, https://doi.org/10.1175/1520-0442(2002)015%3C0386:RSOTAP%3E2.0.CO;2, 2002.

600 Zhou, Z., Nguyen-Xuan, T., Liao, H., Qiu, L., and Im, E.-S.: Characterization of temperature and
601 humidity effects on extreme heat stress under global warming and urban growth in the Pearl and
602 Yangtze River Deltas of China, Weather and Climate Extremes, 44, 100659,
603 https://doi.org/10.1016/j.wace.2024.100659, 2024.

604 Yaglou, C. P. and Minard, D: Control of heat casualties at military training centers, A.M.A. archives
605 of industrial health, 16(4), 302–316, 1957.